A019

Analysis of Coupled and Fully Integrated Models for Low-frequency Electrical Heating Assisted Heavy Oil Recovery

J.A. Torres* (CHLOE), I.I. Bogdanov (CHLOE), V. Dabir (INSA Toulouse) & A. M. Kamp (CHLOE)

SUMMARY

We have studied low frequency heating for heavy oil recovery accompanied by salt water recirculation around electrode wells. The multiphysics nature of this problem naturally calls for a code coupling solution. The main objective of this work is to develop an efficient methodology for such coupling.
We address the coupling paradigm which includes questions about the degree of coupling (with respect to synthesis), grid and solver type used in the simulation of each separate problem, problem stability and accuracy, interpolation strategy, parallelization, etc. The implemented solution was validated and applied.
We coupled a finite volume (FV) reservoir simulator (Stars) to a general purpose finite element (FE) simulator (COMSOL Multiphysics) used to compute an approximation to Maxwell s equations. These two simulators are coupled by an in-house coupler written in Matlab, being its critical step the bi-direction mapping of interpolation/integration of data between the FE and FV mesh. Selection of solver parameters has been confirmed to be critical in order to limit the effect of numerical dispersion.
Coupling solutions, such as the one described in this paper, allow developing simulation tools that reuse as much as possible specialized and existing tools. Their application to practical problems proves to be useful.

Abstract

Simulation of unconventional oil recovery methods may require the development of new numerical tools. This is the case for oil recovery aided by electric heating. The multi-physical nature of this problem naturally calls for a code coupling solution.
Two major problems are addressed in our work. The first one can be formulated as coupling paradigm and includes numerous questions about the degree of coupling (with respect to synthesis in case of fully integrated numerical model), the discretization method(s) and grid(s), the numerical stability and accuracy of a problem, the interpolation strategy, the solver type(s) used in the simulation of each separate problem, the parallelization of computations etc. The second problem is validation and application of the model based on a simulator coupling. The main objective of this work is to develop an efficient methodology for such a coupling. This methodology was applied to modeling of heavy oil recovery based on low frequency heating which is accompanied by water recirculation around electrode wells.
Coupling solutions, such as one described in this paper, allow the development of integral models and their application to practical problems, but also raise new questions concerning an adequate description of the processes under consideration.

Introduction

Exploitation of unconventional hydrocarbon reservoirs becomes more and more challenging activity for energy producing companies throughout the world. Already known and novel approaches should be explored and proposed to provide reasonable technology for such an oil recovery.
Suitable dedicated simulators, however, exist not for each new model and at the exploration period a non-standard approach to numerical modeling and to choice of numerical means can be of great interest. Most frequently a principal idea comes from a non-trivial combination or sequence of known phenomena. In these particular cases a natural choice of numerical modeling tools is a coupling between existing software and simulators. Therefore it is not surprising that the coupling software development has already made its little history (Redler et al. 2009).
Now let's look at the oil recovery aided by electric heating from this viewpoint. The multi-physical nature of the problem is evident. So do its practical importance and limited availability of corresponding modeling tools among the dedicated simulators. All this leads to solutions like coupling models (Koolman et al. 2008, Bogdanov et al. 2008). Thus the first major problem addressed in our paper can be called a coupling paradigm.
Numerous questions to answer concern, for example, the degree of coupling and influence of coupling frequency on numerical solution quality and computational performance of model, discretization method(s) and grid(s), interpolation strategy, solver type(s), parallelization, etc. Few of them have recently been considered in the geomechanical applications framework (Mainguy and Lonquemare 2002, Kim et al. 2009).
Then the second problem concerned here is validation and application of a coupling model. The main objective of this work is to develop an efficient methodology for such a coupling. This methodology has been applied for modeling of low frequency heating (LFH) assisted heavy oil recovery process accompanied by water circulation around electrode wells (cf. McGee and Vermeulen 2007).
We'll couple, indeed, the finite volume (FV) reservoir simulator (CMG STARS) to a general purpose finite element (FE) simulator (COMSOL *Multiphysics*). The latter has been used to compute an alternate electric current field. These two simulators are coupled by an in-house coupler written in MATLAB and called EMIR. The critical step of EMIR proved to be a grid(s) choice (per simulator) and a data mapping (specifically, interpolation/integration) for the data exchange between FE and FV grids. Note that unlike the geomechanical coupling mentioned above, the LFH coupling problem requires finer grid and really gains in performance due to a flexibility in the choice of grid.
Obviously, the different types of discretized model and, consequently, of grid used by simulators never facilitates the task of a coupling tool. Nevertheless, the advantage of coupling may come also from completely separate computations (i.e. separate models) for the equations of different type. For example, the electric potential (elliptic) equation is preferably to solve with the FE method on unstructured grid because of near singular solution in the vicinity of the electrodes, and perhaps so do

the pressure and even the temperature equations. Of course, care should be taken as this may cause some problems of stability and accuracy (cf. Kim et al. 2009) and accordingly, some preliminary work has to be done. In any case, a good practice would be to envisage the coupling possibility from the very beginning of a simulator development.

Low frequency heating: problem formulation

The main idea of electric field implementation is to provide a source of heat inside the reservoir and in this way to facilitate the thermal multiphase flow to production wells. The LFH method has been developing for about thirty years and was already tested at large scale. From the physical viewpoint the method is based on the Joule effect, the original (connate) reservoir water playing a role of conductor. The electrical current is supplied via the electrodes settled directly in the reservoir and the heat is generated over the reservoir volume according to electrical current density and hence the fluid saturation and temperature fields which affect the bulk electrical conductivity (cf. McGee and Vermeulen 2007). An understanding of physical mechanisms of this oil recovery method requires to study the heat and mass transfer under the LFH conditions.

Joule resistive heating

The coupling term between the electric field and multiphase flow equations is the Joule (resistive) heating source which reads as

$$J = \sigma \left| \nabla \upsilon \right|^2 . \tag{1}$$

Here J is the heating power density [W/m3]; σ the bulk electric conductivity [S/m] and υ the (complex) electric potential [V]. The calculation of the bulk electrical conductivity (σ) is important point in this study since it depends on (multiphase) fluid composition and temperature, and thus explicitly couples the variables of electric field and the thermal flow model. The modified formulation of Archie's law which takes into account the temperature dependency (factor f(T)) is used in current work:

$$\sigma = \sigma_w \varepsilon^m S_w^n f(T) . \tag{2}$$

Here σ_w is pure water electric conductivity at reference temperature, ε medium porosity, S_w water (local) saturation, m and n the constant parameters. The temperature dependency can be approximately presented by linear function which increases the conductivity by a factor of 3 to 4 for a temperature increase of 100°C (McGee and Vermeulen 2007)).
In the case of complex electric potential (*eg* using an industrial three-phase current system), υ=φ+iψ, the electric charge conservation law may be written as a system of two stationary equations for real and imaginary potential parts:

$$\nabla \cdot \left(\sigma \nabla \varphi \right) = 0 \tag{3}^a$$

$$\nabla \cdot \left(\sigma \nabla \psi \right) = 0 . \tag{3}^b$$

The Joule heat release is then defined by the equation (1) where

$$\left| \nabla \upsilon \right|^2 = \left(\nabla \varphi \right)^2 + \left(\nabla \psi \right)^2 , \tag{4}$$

and the bulk medium electric conductivity σ is a dependent variable according to Archie's law (2). In particular, this means that the heating source (J) is solution dependent and there is a strong coupling between electrical and thermal flow phenomena. In particular, this non-linear coupling leads to the temperature rise acceleration during LFH. The equations above either complement the fully integrated CMG STARS model of the thermal flow (see below) or offer a COMSOL LFH model for the EMIR computations.

Thermal three-phase flow

The thermal flow model equations include the fluid component mass and the total thermal energy conservation equations. The mass conservation equations are written for the water component which

is either a liquid (index "w") or a water vapor ("g"), and the oil which is assumed to be uniform non-volatile hydrocarbon liquid (index "h"). Then the equations read as

$$\partial_t\left[\varepsilon\left(\rho_w S_w + \rho_g S_g\right)\right] + \nabla\cdot\left(\rho_w u_w + \rho_g u_g\right) = 0 \tag{5}$$

$$\partial_t\left(\varepsilon\rho_h S_h\right) + \nabla\cdot\left(\rho_h u_h\right) = 0 \tag{6}$$

where phase flows u_p, p=w,g,h, are described by generalized Darcy' law

$$u_p = -K\eta_p\cdot\left(\nabla P_p + \rho g e_z\right) \tag{7}$$

Here K is absolute permeability, ρ and η phase density and relative mobility, S phase saturation. As the temperature is not uniform in the reservoir, the total thermal energy conservation equation which includes solid (index "s") and fluid (index "f") phases contributions under assumption of local thermal equilibrium (one-temperature approach), complements the model

$$\partial_t\left(E_s + E_f\right) + \nabla\cdot\left(U_f - \lambda\nabla T\right) = J\,, \tag{8}$$

where E is volumetric internal energy, U_f total volumetric flow of thermal energy, λ reservoir (bulk) thermal conductivity coefficient, T reservoir temperature. The total flow U_f comprises fluid phase flows, $U_p = \rho_p h_p u_p$, p=w,g,h, where h is phase specific enthalpy.
Finally, the pore volume saturation constraints phase saturations in usual manner

$$S_g + S_w + S_h = 1\,. \tag{9}$$

The constitutive pressure-saturation-permeability relations together with fluid physical properties variation with temperature and pressure complete the above system of model equations. Typical values of physical properties and material functions used in the LFH modeling for bitumen reservoir can be found in Table 1. For more details about the input data see Bogdanov et al. (2010).
Note first that the stationary electric field equation (3) depends parametrically on time so that the coupling time step that may normally include numerous time steps of STARS is still limited.
Note further that the coupling term (equations (1),(8)) doesn't depend on spatial derivatives of flow variables. This simplifies considerably the linear analysis of numerical stability for coupling model.

Fully integrated and coupling models

As it has been mentioned above, in case of LFH the two distinct but interrelated physics are resolved: the thermal multiphase flow through porous media, and the electrical current distribution. Two models have been used to solve the LFH equations: the CMG STARS fully integrated model (FIM) which includes the electric module application or simulator coupling tool EMIR (CM) based on COSMOL *Script* and MATLAB utilities.

Approach STARS

The electrical heating model of STARS (STARS-LF) was used as a FIM to solve for electrical field and thermal flow equations in the reservoir. Electrical conductivity is defined by the Archie's law extension taking into account the temperature dependency (equation (2)). To facilitate the convergence procedure on each Newton's iteration the electric heating rate is maintained constant. In this work, two types of boundary conditions were used as electrical operational constraints: the maximum electric potential magnitude given on electrodes or the maximum total instantaneous resistive heating power. Note that, generally speaking, the boundary conditions for electric field model are given in slightly different way in STARS-LF and COMSOL so that care should be taken to make them as similar as possible.

Approach EMIR

The coupling model (CM) was built using an in-house code called EMIR. It follows a loose coupling algorithm which implies that the thermal flow and the electric field models are solved sequentially, with separate solvers. EMIR was written in MATLAB and its main function consists in controlling

the sequential computations performed by two dedicated simulators. A finite volume simulator, CMG STARS, solves the energy and component transport problem while a finite element simulator, COMSOL *Multiphysics*, computes instantaneous heating power distribution. Evidently, both solutions undergo certain transformations (interpolation/integration) which may influence the numerical solution in non-trivial way. On the other hand, the CMG STARS based fully integrated model (see above) was extensively used for EMIR validation purposes.
The main steps during EMIR computations are organized as following. The model parameters (see Table 1) are initialized and the sequential loop is started by solving first the electric field model. The Joule power density is computed (on COMSOL FE grid, normally, unstructured) before its spatial integration over each block of STARS FV grid (structured, rectangular or hexahedron). Upon termination of the coupling term computation and output the next reservoir simulation step begins via launching STARS computations. The new electrical conductivity field is computed. Mapping of necessary reservoir variables is carried out with the aid of EMIR interpolation utilities which input FV grid data and transforms them for subsequent use on FE grid. This loop is repeated at each coupling step until the final time is reached. It can be seen easily that EMIR results may be influenced by numerous numerical parameters, such as spatial discretization (of both FE and FV grids) or time discretization and in particular, the coupling frequency (coupling time step).

Coupling model verification and validation

Numerical stability and accuracy

As each simulator controls independently the numerical solution, the problem to be investigated reduces to examination of coupling r.h.s. term (1) (see also (8)) and its possible temporal and spatial discretization. The linear stability analysis becomes self-evident as the coupling r.h.s. term (1) does not include the spatial derivatives of flow variables. Finally, it results in demonstration that possible problem may come rather from solution accuracy which really depends on the coupling frequency and shows progressive deviation at lower frequency (Figure 5). No critical behavior of the discretized CM has been detected during numerous tests which included large variations of coupling time step and spatial discretization lengths.

Comparison to analytical solutions

Other approaches used for the model validation included:

- direct comparison to available analytical solutions;
- juxtaposition of EMIR and STARS computation results;
- energy balance computations;
- analysis of grid global refinement and choice of FE order and their influence.

For the sake of facilitating the derivation of exact solution the initial problem has been reduced to heat transfer with single phase stationary flow under conditions of the LFH in a uniform porous medium. It can be shown that the dimensionless problem for 1D radial case is described by following equation

$$\theta_\tau + \frac{\Pi}{\rho}\nabla\theta - \Delta\theta = \frac{1}{\rho^2} \tag{10}$$

which applies for dimensionless radial distance $\rho_0 \le \rho \le 1$. Here the dimensionless variables are introduced as follows: θ is temperature, τ time, Π the thermal Peclet number. Analytical solutions have been developed for the conduction and convection/conduction heat transfer in uniform or composite medium using stationary boundary conditions for applied potential, temperature and/or no conduction heat flow at the inner (electrode radius ρ_0) and outer boundaries, $\rho = \rho_{0,1}$.
In Figure 1 the results of the reservoir preheating (see case 1 below) by Joule power during 1 year are shown. The bulk electrical conductivity was uniform and constant. Comparison between EMIR, the FIM and the analytical solution of (10) shows very good agreement. Similar problem of LF heating but with single finite electrode (case 2 below) and for case with water circulation around it (to prevent the connate water evaporation) was used to check the FIM and the CM numerical solutions. The simulations have been done in 3D; the results of STARS to EMIR comparison demonstrate once more

a good agreement; note that STARS used radial structured grid which is perfectly adapted to the problem geometry unlike the non-structured tetrahedral COMSOL grid.

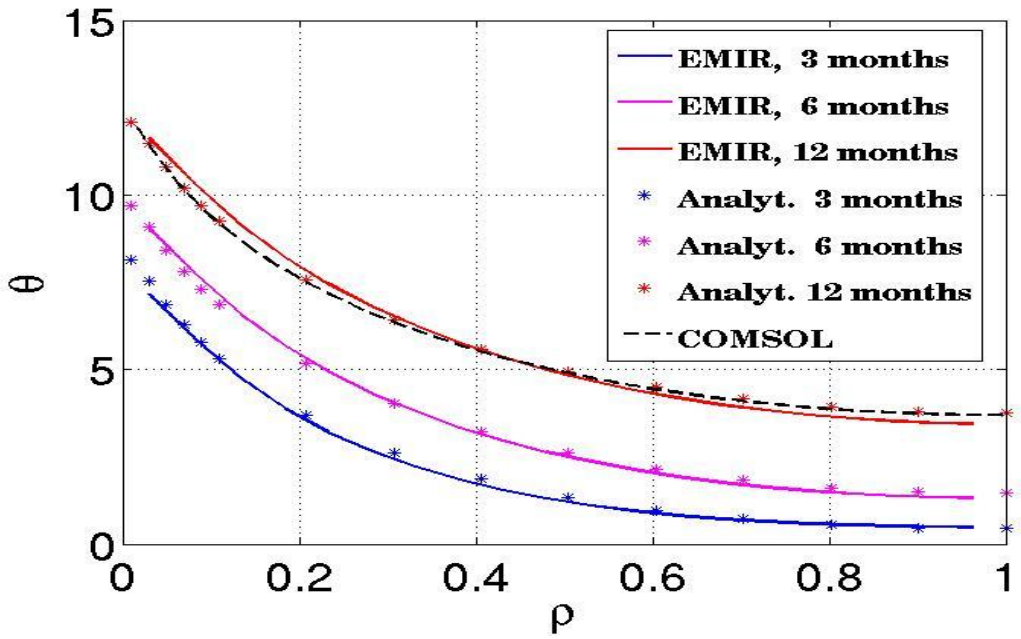

Figure 1. Case 1: EMIR and STARS numerical solutions comparison to analytical solution.

Main results and discussion

The coupling (EMIR) and the fully integrated (STARS-LF) models were used for two-case study of the LFH around single electrode. The modeling results were compared and analyzed. First of them is a case of LFH radial model without injection/production (constant fluid saturations). The two major assumptions for this model were: the infinite electrode and the linear variation of electrical conductivity with temperature. Then, a 2D axisymmetric model of LFH with finite electrode and salted water circulation around it was used to study the temperature field variation around the electrode (case 2). The salted water circulation modifies significantly the electrical conductivity, so that the influence of coupling time step becomes more important.

Table 1. Main parameters of base cases simulations.

	Case 1	Case 2	Units
Reservoir length	8	8	M
Reservoir height	13	13	m
Electrode length	7	7	m
Electrode radius	0.1	0.1	m
Electrode potential	100	220	V
Production bottom hole pressure	8.0	8.0	bar
Injection bottom hole pressure	-	15	bar
Initial reservoir temperature	10	10	°C
Initial reservoir pressure	10	10	bar
Initial water saturation	20	20	%
Initial oil saturation	80	80	%
Initial reservoir salt concentration	0.5	0.5	%wt
Injected salt concentration	-	5.0	%wt
Eff. initial bulk electrical conductivity	0.088	0.005	S/m
Initial oil viscosity	147.2	1000	Pa·s

Besides, the sensitivity to STARS grid block size was checked for both cases. Table 1 lists the main model parameters and reservoir properties, the electrode and the well operational conditions. Table 2 presents and classifies the different grids studied and Figure 2 illustrates the problem formulations (Figure 2a) and two structured rectangular STARS FV grids (R2 and R32) with their COMSOL FE triangular unstructured "counterparts" (Figure 2b,c). The total number of degrees of freedom used by COMSOL are in the range 2-9·104, approximately (cf. Table 2). Preliminary computations were made to adapt a relatively dense COMSOL mesh for each case and to check the influence of this parameter on numerical solution.
The COMSOL discretized model was based on numerous sub-domains each of which is identical to a corresponding FV grid block, with so-called internal boundaries between them. It allows to control more effectively both a triangular grid generation (done with advancing front technique) and a computation of power integrals per FV grid block.

Table 2. Cases 1 and 2 Grids and discretization parameters for cases 1 (a) 2 (b) models.

(a)

Grid type	Coarsest	Coarser	Coarse	Medium	Fine	Finer
Grid name	R02	R04	R08	R16	R32	R80
Δx, m	4.0	2.0	1.0	0.5	0.25	0.10
No DOF	68954	19554	77506	20802	57858	154402
h_M	0.12	0.23	0.12	0.25	0.19	0.10
No. elements	17070	4800	19200	5120	14336	38400

(b)

Grid type	Coarsest	Coarse	Fine
Grid name	R12	R24	R36
Δx, m	0.67	0.33	0.222
Δz, m	1.0	0.5	0.333
No DOF	71194	48494	109318
h_M	0.15	0.14	0.10
No elements	17784	6124	27144
P_{inj}, bar	13.5	15.0	16.2

Case 1

This case considers the preheating period without any fluid injection or production. Figure 3 shows a comparison between results obtained with EMIR using four grids (R04, R16, R32 and R80) against the finest STARS grid, R80. The maximum temperature after 30 days of preheating (Figure 3a) is always below the saturation temperature, and there is no steam in reservoir at this time. On the other hand, the total power delivered to the reservoir augments progressively until 30 kW (Figure 3b). Both maximum temperature and total power time diagrams indicate a perfect match between the FIM and the CM when using the fine grid. Later, the comparison between different grid results (cf. R04, R16 and R32) indicates an underestimation of the maximum temperature on progressively coarser grid. Maximum temperature can be observed, normally, in the close electrode vicinity where the power density is great (nearly singular); so may be expected the difference of mean temperature over a grid block at different spatial discretization. The use of a coarse grid (such as R04, for instance) produces a significant difference of approximately 16% in terms of total power density after the preheating period.
Figure 4 shows the grid sensitivity for the CM (EMIR) at different STARS grids, after 10 days of pre-heating. The compared factors include average and local power density, temperature and electrical conductivity profiles observed on the STARS grid. The average power density corresponds to the value assigned at each FV grid block; while the local power density matches the value computed in the FE grid. The FIM and the CM gave the same results when fine grids are used. The average power

density profile on the STARS blocks (Figure 4a) illustrates that the coarser grid (R4) cannot represent adequately the elevated temperatures in the proximity of the electrode, i.e. inside a distance lower that 1m from the electrode.

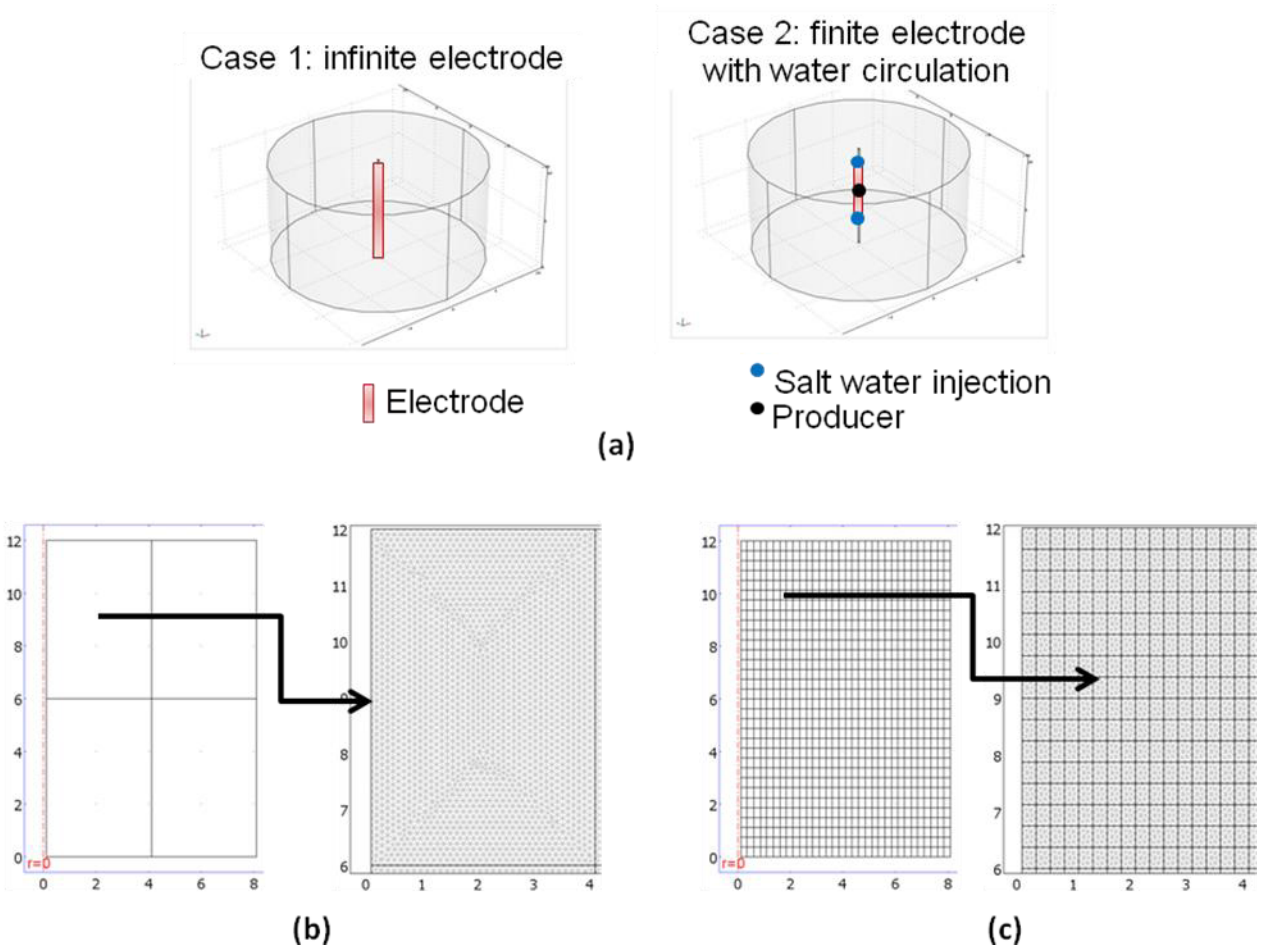

Figure 2. Problem formulations and grid examples.

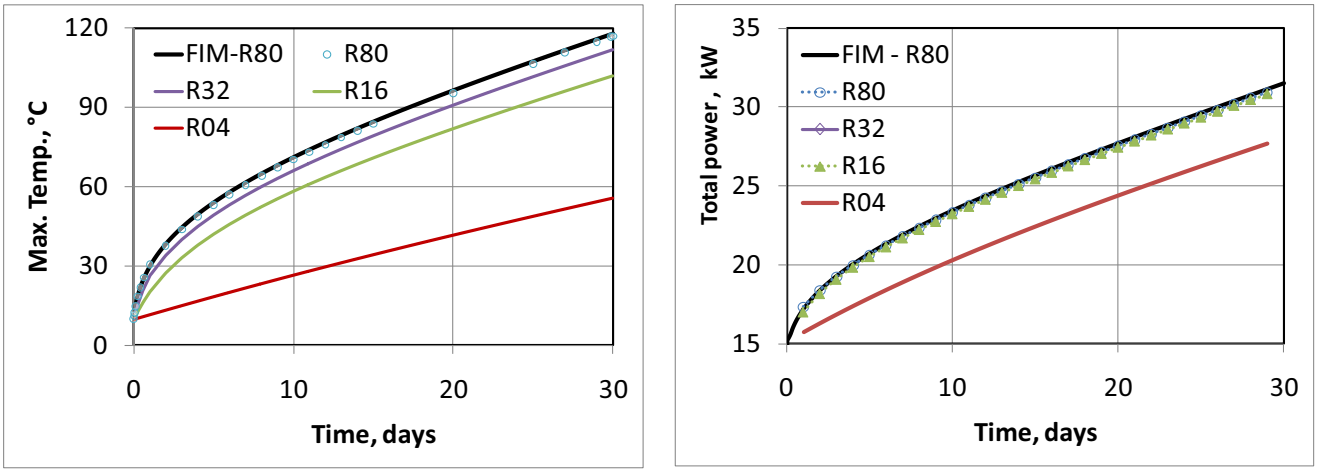

Figure 3. Comparison of models for case 1: the CM at different FV grid to the FIM results at fine grid (R80).

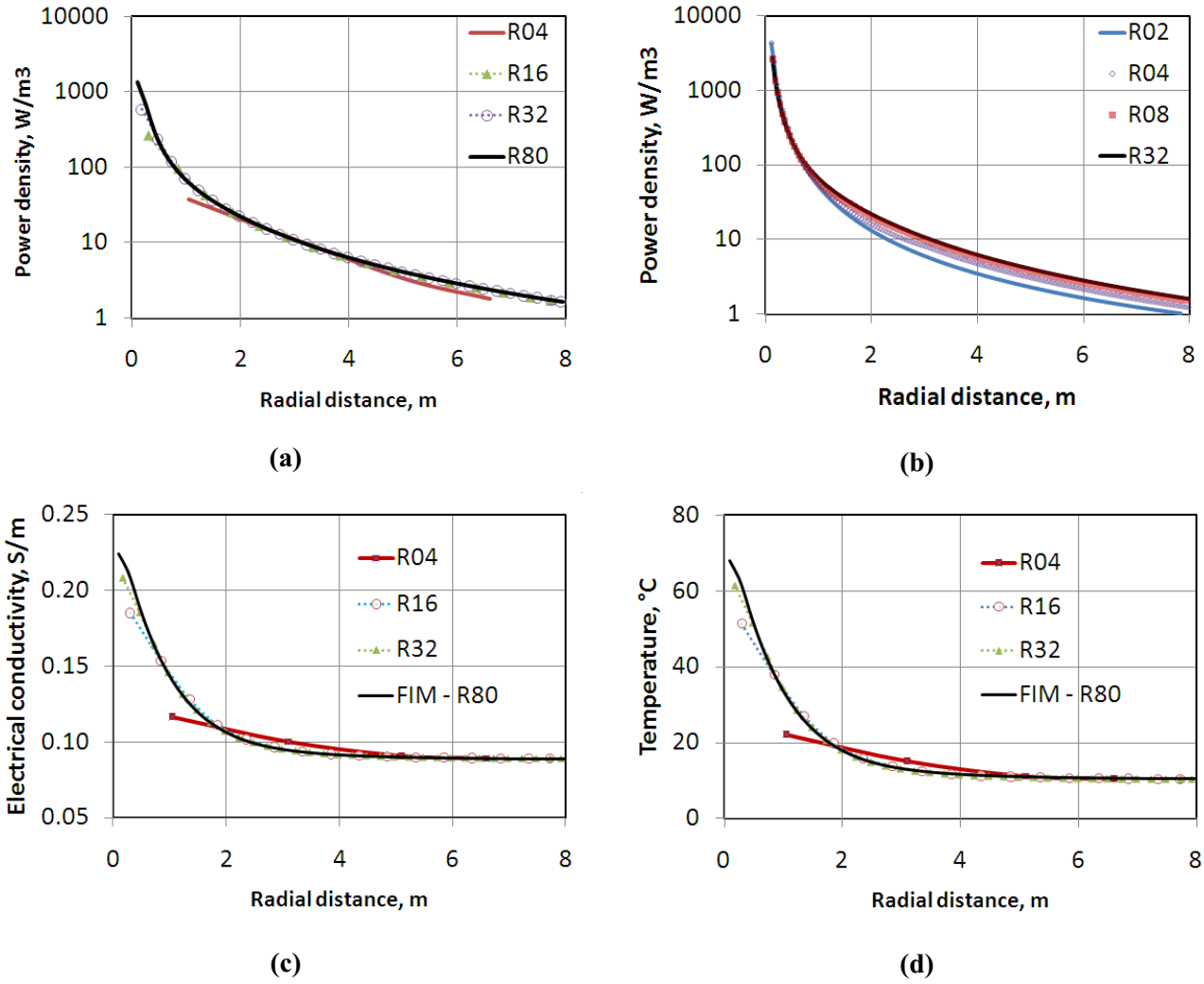

Figure 4. Sensitivity of results to grid size for case 1.

Alternatively, the local power density profile (Figure 4b) demonstrates that the use of a fine FE grid gives a continuous profile even for a coarse underlying FV grid. After refinement of the STARS grid, power density converges to the fine grid value (R80). Main factor in this difference is the electrical conductivity field which is a function of temperature. Comparison between the electrical conductivity fields for a coarse grid and a fine grid (Figure 4c) demonstrates a significant difference (of about 50%) of the maximum values of electrical conductivity for the coarser grid, which also is locally higher around the electrode.

To conclude the one-dimensional FIM and CM gave identical results when fine grids are used. For the CM, the selection of a fine COMSOL mesh helped much to provide an adequate solution of the electrical problem. Sensitivity to the STARS grid demonstrated that an accurate reproduction of the temperature field in the vicinities of the electrodes requires the use of small size blocks.

Case 2

Case 2D comprises a study of the preheating period when a water circulation regime is established around the electrode body. This operation has a double purpose: to reduce the electrode temperature

and to avoid the hot spots, and to accelerate heat transfer from the electrode to the reservoir. Two injection points are located at the extremities of the electrode and one production point is located at the electrode center. Salted water is injected which increases the bulk electric conductivity and facilitate the electrical current flow. Remind that bulk electrical conductivity is a function of four variables (Archie's law, equation (2)): water phase saturation, salt concentration, temperature, and porosity. Results obtained during the study allowed to compare the CM and the FIM solutions, and to analyze the sensitivity to FV grid block size and to coupling time step.

In particular, Figure 5 shows the influence of the coupling time step on the maximum temperature and the cumulated energy delivered to the reservoir. Five values of coupling time step have been involved, all in the range from 6 to 96 hours. In general, the difference between the STARS reference solution and the EMIR solution is satisfactory at all coupling time steps except for one (96 hours). Curiously, the most sensitive variable in this test turned out to be the maximum temperature at initial times; its relatively large deviations took place because of the relatively fast modification of the properties field (water saturation, salt concentration…) imposed by the salted water circulation.

Figure 6 compares the time profile of the total power delivered to the reservoir and the maximum temperature for STARS grid, R12 and R36. Note that the injection pressure was modified to compensate the variation of well index affected by geometrical factors at different block sizes. In general, both parameters match reasonably well, still the best being the results on the finer grid (R36). The relative error in terms of the total power after 30 days of preheating is approximately 4% for R36 and 11% for R12; which confirms the better precision of the finer grid.

Figure 7 juxtaposes the computed power density after 30 days of preheating for two FV grids: R12 on the left column and R36 on the right column. Shown in the top row (Figures 7a and 7b) are the average power densities obtained per each FV grid block during the coupled simulation while in the middle row (Figures 7c and 7d) are plotted the local power density computed on the COMSOL mesh. It is clear that the finer is FV grid, the better resolution can be obtained in the average power field. On the other hand, after comparison of top and middle plots, it becomes evident that some part of information from FE grid is lost during "upscaling" done for each FV grid block.

Figures 7e and 7f show the relative difference in electrical power fields computed per grid block for R12 and R36 grids using FIM (FV structured grid) and corresponding CM (FE triangular grid with post-integration of the field over each FV grid block). The difference is calculated like conventional relative error, so that positive values indicate that the CM solution is greater than the FIM solution, which is the case for the major part of the blocks. Note that in the region close to the boundary of water circulation chamber (around electrode) where the bulk electrical conductivity drastically changes, the (negative) relative difference is more significant. This indicates clearly that finer triangular grid gives more reliable results in the vicinity of electrical properties interface. Another singular region where the local deviation is relatively high is in the vicinity of the injection points, the top and the bottom ones. There are two singular blocks at the left top and bottom corners where the electrical power is relatively low because of nearly zero electrical current.

Conclusions

- a good agreement between the coupling model (EMIR) and the fully integrated model (CMG STARS) results was obtained for two considered cases of the LFH assisted oil recovery;
- the FE grid used by the coupling model is more flexible and offers better geometrical and thus numerical problem description;
- the coupling model is still sensitive to the grid block sizes and relatively fine FE grid should be used in order to limit the local numerical dispersion of the computed power;
- the strong variation of bulk electrical conductivity with a porous medium state and specifically, with water saturation and concentration of a salt, constraints the coupling time step especially in the situation of relatively fast evolution of electrical properties around electrodes.

Acknowledgements

TOTAL company is gratefully acknowledged for having sponsored our research work.

References

Bogdanov, I.I., El Ganaoui, K., Kamp, A.M. [2008] Study of Electric Heating Application for Heavy Oil Recovery, European COMSOL Conference 2008, Hannover, Germany.

Bogdanov, I.I., Torres, J.-A., Akhlaghi, H., Kamp, A.M. [2010] The Influence of Salt Concentration in Injected Water on Low Frequency Electrical-Heating Assisted Bitumen Recovery, SPE129909-PP paper presented at SPE Seventeenth Symposium on IOR held in Tulsa, OK, 24-28 April, 2010.

Kim, J., Tchelepi, H.A., Juanes, R. [2009] Stability, Accuracy and Efficiency of Sequential Methods for Coupled Flow and Geomechanics, SPE 119084, 20pp.

Koolman, M., Huber, N., Diehl, D., Wacker, B. [2008] Electromagnetic Heating Method to Improve Steam Assisted Gravity Drainage, SPE/PS/CHOA International Thermal Operations and Heavy Oil Symposium, 20-23 October 2008, Calgary, Alberta, Canada

Mainguy, M. and Longuemare, P. [2002] Coupling fluid flow and rock mechanics: formulations of the partial coupling between reservoir and geomechanical simulators, Oil & gas science and technology –Rev. IFP, 57, No.4, pp. 355-367.

McGee, B.C.W., Vermeulen, F.E. [2007] The Mechanisms of Electrical Heating for the Recovery of Bitumen From Oil Sands, Journal of Canadian Petroleum Technology, **46**, No.1, pp.1-7.

Redler, R., Valcke, S., Ritzdorf, H. [2009] OASIS4 – a coupling software for next generation earth system modeling, Geosci. Model Dev. Discuss., **2**, pp.797-843.

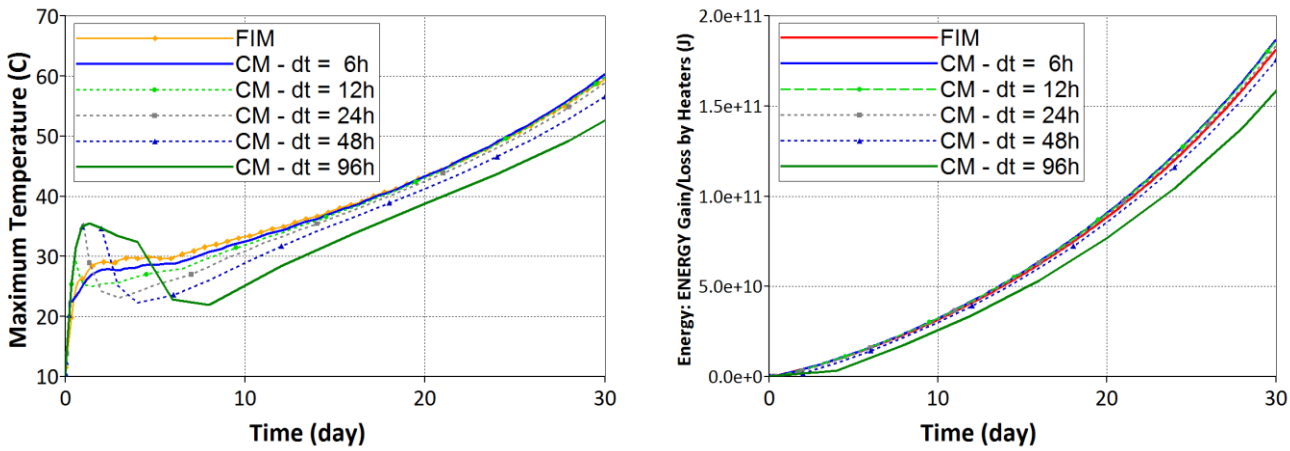

Figure 5. Sensitivity of case 2 results to coupling time step.

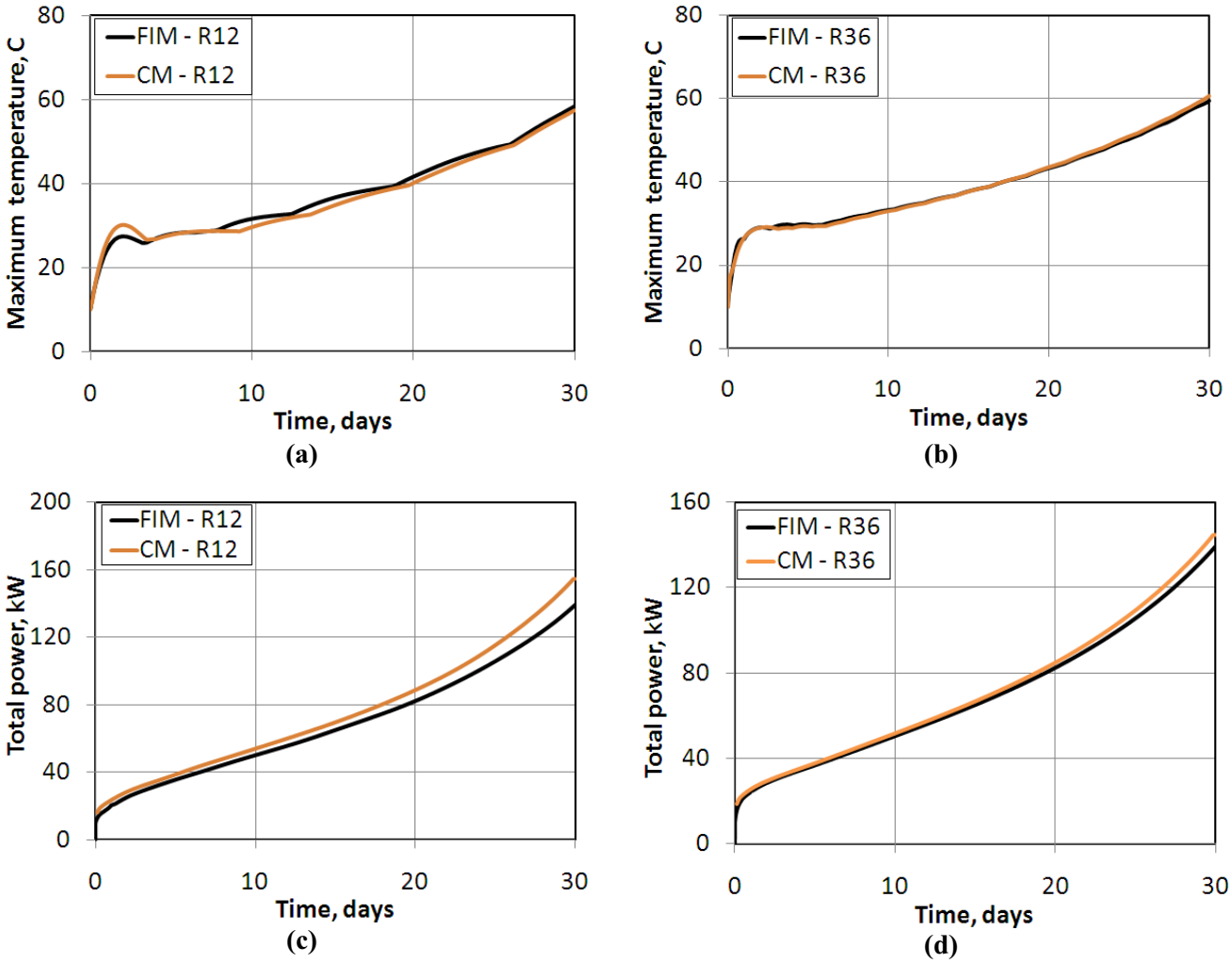

Figure 6. Case 2: comparison of results for two different FV grids.

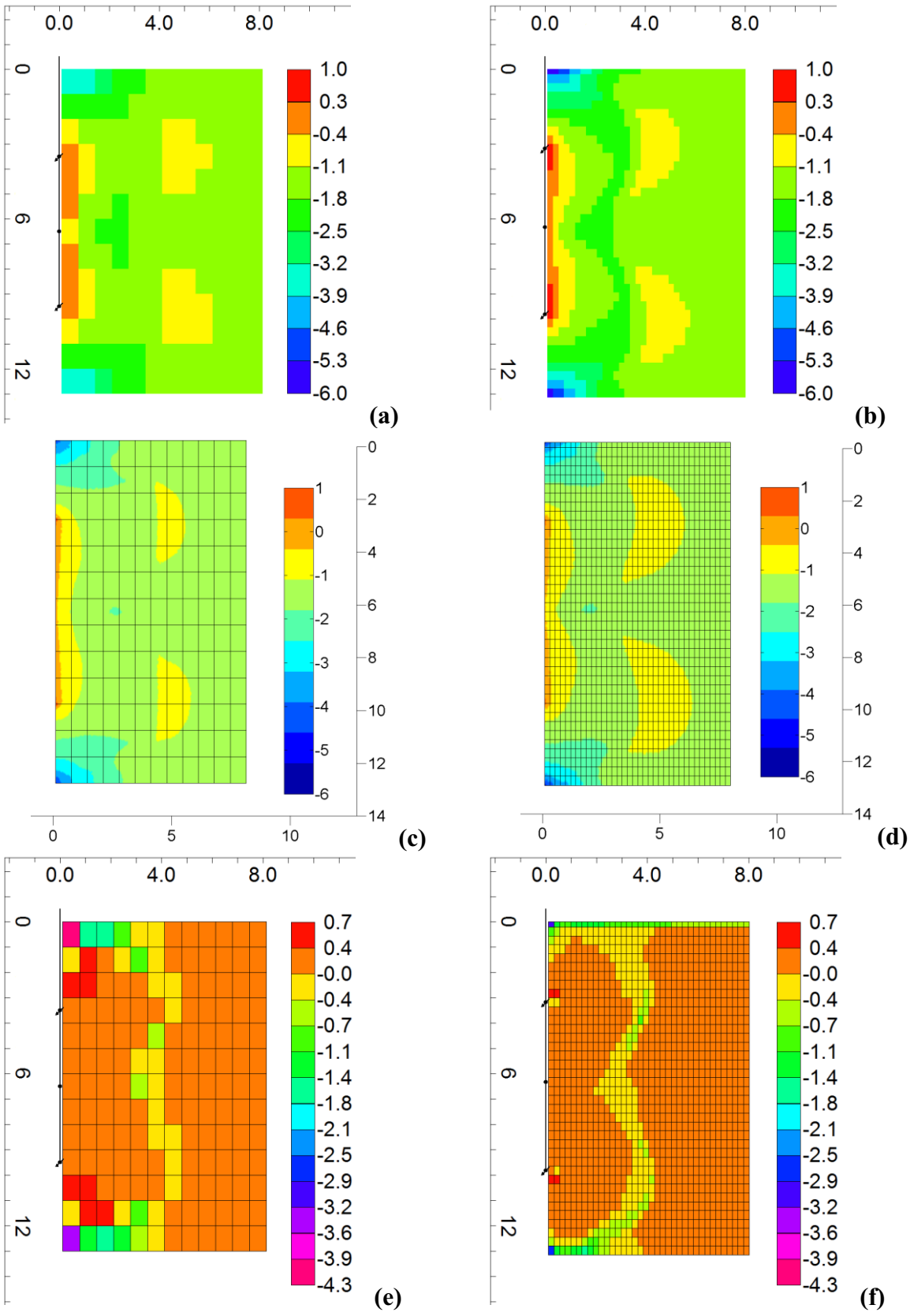

Figure 7. Case 2: sensitivity to FV grid block size.